ELSEVIER

Mechanics of Materials 29 (1998) 219–232

MECHANICS OF MATERIALS

Recent developments in velocity and stress measurements applied to the dynamic characterization of brittle materials

Horacio Dante Espinosa [1]

Purdue University, West Lafayette, IN 47907-1282, USA

Received 11 August 1997; revised version received 15 December 1997

Abstract

The synthesis of novel brittle materials with tailored microstructures requires the understanding of new physical phenomena related to the failure of these materials. Observation capabilities with spatial resolution of atomic dimensions, e.g., scanning tunneling microscopy (STM) and high resolution electron microscopy (HREM), have opened new frontiers in the mechanical characterization of these advanced materials. The challenge is to design experiments capable of loading the material in a controlled fashion such that defects, resulting in well defined macroscopic stress and velocity features, are produced. In this article, techniques for the measurement of surface and in-material particle velocities and in-material axial and transverse stress measurements are reviewed. Examples on the usefulness of these techniques in the study of brittle failure are provided. A variable sensitivity displacement interferometer is used in the measurement of normal and in-plane motion in pressure–shear recovery experiments conducted on fiber composite materials. In-material stress measurements with piezoresistance gauges are used in the identification of so-called failure waves in glasses.

Keywords: Interferometry; Wave propagation; Failure mechanisms; Inelasticity; High strain rate

1. Introduction

Experimental techniques that allow the identification and modeling of failure from a micromechanical standpoint are currently available. They consist in wave propagation experiments which utilize diagnostic tools possessing the spatial and temporal resolution for resolving features related to the failure processes. For instance, laser interferometry for point and full field measurements, with a resolution of 1 ns and a few micrometers, is a powerful tool currently in use in wave propagation studies. These studies can be designed to identify existing damage or inelasticity in the material without further generation or modification of microdefects, or they can be designed to initiate and accumulate inelasticity within the material in a controlled fashion. The first class of wave propagation experiments falls into the subject of nondestructive evaluation of material systems. The latest are wave propagation experiments, e.g., impact experiments, resulting in extensive microstructural modification within the specimen. A variety of configurations exist in which plates and rods are utilized. Here we will discuss in some detail plate on plate impact experiments to illustrate the applicability of the velocity and in-material stress measurement techniques. The reader should note that the theory presented is completely general.

[1] E-mail: espinosa@ecn.purdue.edu.

PII: S 0 1 6 7 - 6 6 3 6 (9 8) 0 0 0 1 6 - 7

Plate impact experiments are essentially wave propagation experiments which have been successfully employed in studies of microplasticity (Kumar and Clifton, 1979), high strain rate properties of metals (Clifton and Klopp, 1985), microcracking (Espinosa and Clifton, 1991), rheological properties of lubricants (Ramesh and Clifton, 1987), and material instabilities (Zhou et al., 1994). The experimental technique consists of launching a flyer plate against a target plate using a light gas gun. Normal and shear waves, with a time resolution of a few nanoseconds and magnitudes up to several gigapascals (GPa), are generated within the plates upon impact. A schematic of the pressure–shear *recovery* impact experiment is shown in Fig. 1(a). Elastic wave fronts for a plane wave analysis of a high strain rate pressure–shear recovery experiment, in a Lagrangian *X–t* diagram, are shown in Fig. 1(b). At impact, plane compression waves and shear waves are produced in both the impactor and the target. Since the shear wave velocity is approximately half the longitudinal wave velocity, a thin film with very low shear resistance needs to be added to the flyer plate such that the arrival of the unloading shear wave to the impact surface precedes the arrival of the unloading longitudinal wave generated at the back surface of the second flyer plate. The thickness of the target plate must be selected so that the arrival of longitudinal unloading to the impact surface, from the target back surface, does not prevent the transfer of the main shear pulse to the target plate.

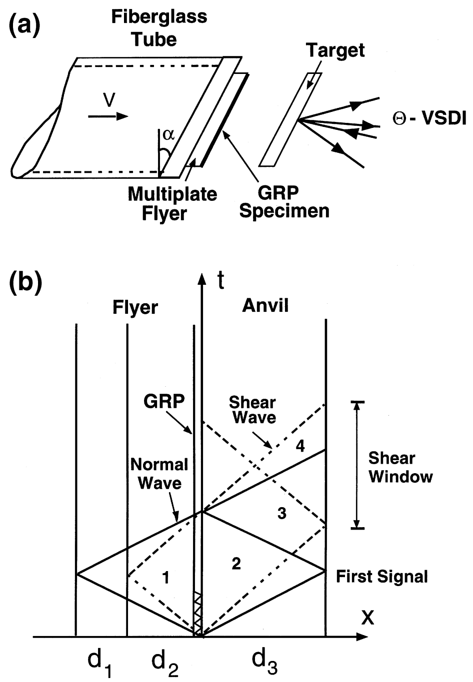

Fig. 1. (a) Schematic of high strain rate pressure–shear configuration. (b) Lagrangian *X–t* diagram for the case of pressure–shear recovery experiment.

In the case of recovery experiments (Espinosa and Clifton, 1991; Espinosa, 1992; Espinosa et al., 1992, 1997a; Machcha and Nemat-Nasser, 1994, 1996; Yadav et al., 1993), postmortem examination of the specimens, by means of SEM, TEM and other observational methodologies, allows the identification of failure mechanisms. These observations form the bases for (i) the comprehensive understanding of the processes occurring during material deformation and (ii) the formulation of physically based constitutive models. Interferometric records, obtained during the wave propagation event, are used as a diagnostic tool in the examination of derived or postulated models. The resolution and location, free surface or in-material, of these measurements are essential to the identification process.

2. Surface velocity measurements with laser interferometric techniques

Laser interferometry has proven to be a highly reliable and accurate means for measuring particle motion in wave propagation experiments. Particle velocity histories were initially monitored in wave propagation experiments by means of a normal velocity interferometer (NVI) developed by Barker and Hollenbach (1965). In this technique, normally reflected laser light from the target plate is collected and split into two separate beams which are subsequently interfered after traveling through different path lengths. The interferometer's sensitivity is a function of the delay time τ between the interfering beams, and the resulting fringe signal is related directly to changes in normal particle velocity.

Barker and Hollenbach (1972) introduced a significantly improved NVI system termed VISAR (velocity interferometer for any reflecting surface). The VISAR was developed by using the wide angle Michelson interferometer (WAM) concept, resulting in an interferometer capable of velocity measurements from either a spectrally or diffusely reflecting specimen surface. Another improvement incorporated into the VISAR was the simultaneous monitoring of two fringe signals 90° out of phase. A schematic of the light path in a fiber optic VISAR with adjustable air delay leg is shown in Fig. 2. Laser light is transported to the back surface of target plate by means of a fiber optic probe manufactured by Valyn International. Lenses 1 and 2 are used to form an image of Retroreflector/PZT (M3) at M3′ such that M1 and M3′ appear coincident when viewed from the detectors. The polarizer beam splitter, after the collimator, is used to generate a diagnostic beam and to polarize the light transported by the 300 μm core diameter fiber. The $\lambda/2$ wave plate is used to rotate the light polarization axis while the $\lambda/4$ wave plate is utilized to retard the P-light component by a phase angle of 90°. Detector outputs $A(t)$ and $A'(t)$ and $B(t)$ and $B'(t)$ are subtracted by a differential amplifier not shown in the figure. The output from the differential amplifiers is recorded in a 1 GHz bandwidth oscilloscope. Quadrature coding is obtained by adding a quarter-wave retardation plate and two polarizing beam splitters. It eliminates ambiguity in the sign of the acceleration and improves accuracy when data reduction is performed using the high resolution regions of the traces. In most VISAR systems, three signals are recorded, the two quadrature optical signals obtained from horizontally and vertically polarized components of light that differ in phase because of the retardation plate, plus the intensity monitoring signal used in data reduction. However, higher signal-to-noise ratios can be obtained by subtracting the two s-polarized beams and the two p-polarized beams, both pairs 180° out-of-phase (Hemsing, 1979). This feature known as push–pull significantly reduces the noise introduced by incoherent light entering the interferometer. The VISAR has been successfully used to monitor normal particle velocity histories in shock wave experiments for over two decades and remains a principal tool of the field.

Another laser interferometer to emerge in that decade was the LDV or laser Doppler velocimeter

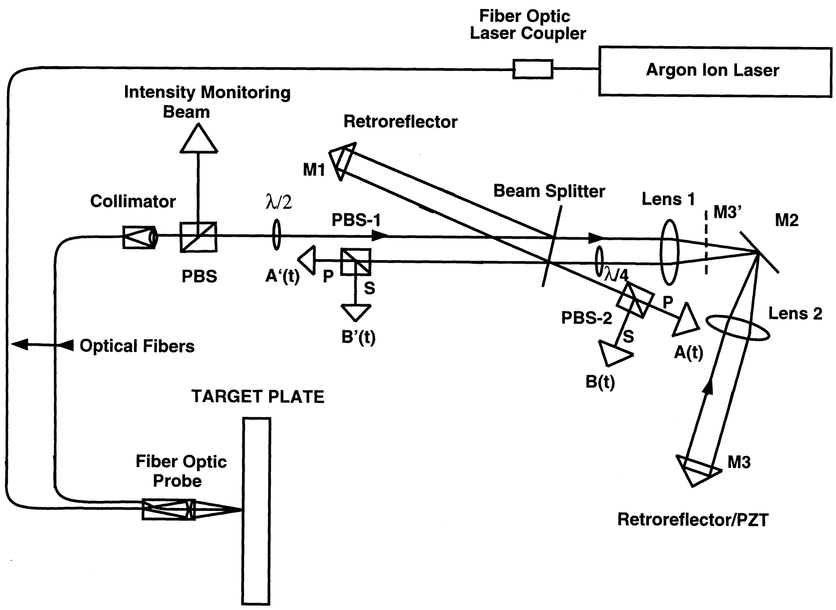

Fig. 2. VISAR interferometer with air delay leg and fiber optics to transport the laser light.

developed by Sullivan and Ezekiel (1974). The LDV can be used to monitor in-plane motion but does not lend itself to the simultaneous monitoring of normal motion. The need to measure both normal and in-plane displacements prompted the development of the TDI (transverse displacement interferometer) by Kim et al. (1977). The TDI takes advantage of diffracted laser beams generated by a grating deposited or etched onto the specimen rear surface. In this technique, the zeroeth order reflected beam is used to monitor longitudinal motion in a conventional way by means of an NVI, or NDI (normal displacement interferometer) while any pair of nth order symmetrically diffracted beams may be interfered to obtain a direct measure of the transverse particle displacement history. The sensitivity of the TDI is given by $1/2\sigma n$ [mm/fringe] where σ is the grating frequency and n represents the order of the interfering diffracted beams.

Chhabildas et al. (1979) presented an alternative interferometric technique particularly suited for monitoring in-plane particle velocities in shock wave experiments. The technique employs two VISARs which monitor specific diffracted laser beams from a target surface. Since one or both of the resulting signals contains a linear combination of the normal and in-plane components of surface motion, it is always possible to decouple the transverse velocity from the normal velocity through a linear combination of the two fringe records.

Both techniques, the two-VISAR and the NDI–TDI, have advantages and disadvantages. The combined NDI–TDI system has a much better resolution at low velocities, but requires the deposition of grids on the free surface of the target plate. On the other hand, the two-VISAR technique provides velocity profiles directly without the need to differentiate displacement profiles. Although the two-VISAR technique is simpler to use when optical windows are needed, it was shown (Espinosa, 1996) that a combined NVI–TDI with window interferometer is feasible. In contrast to the embedded electromagnetic gauge technique to measure velocity histories, both of these interferometers can be applied to a wide variety of materials, metallic or nonmetallic. Moreover, the noncontact feature of the measurement system makes these techniques ideal for high temperature studies of materials.

The development of the NVI was motivated by the relatively small range of velocities that can be measured by the NDI. The latter interferometer is a derivative of the original Michelson interferometer in which a light beam reflected from a moving target is interfered at a beam splitter with a stationary reference beam. The sensitivity of the NDI is given by $\lambda/2$ [mm/fringe] where λ represents the laser light wavelength. The extreme sensitivity of this interferometer severely limits its application in wave propagation experiments due to the inordinately high signal frequencies which may be generated.

An NVI or a VISAR on the other hand, has a variable sensitivity given by $\lambda/(2\tau(1+\delta))$ [mm/μs/fringe] whereby τ represents a time delay between the interfering light beams introduced by an air delay leg or etalon in the interferometer. The factor $(1 + \delta)$ is a correction term to account for the refractive index of the etalon. A quite appealing feature of this interferometer is that the fringe record is a direct measure of particle velocity, thereby alleviating the need for differentiation of the reduced signal. Moreover, signal frequencies generated by an NVI are proportional to particle acceleration and are therefore lower than equivalent signal frequencies generated by an NDI. However, during an initial time period τ, an NVI is functioning as an NDI since the delayed light arriving at the detector from the delay leg or etalon is reflected from a stationary target (Clifton, 1970). Ironically, it is the interpretation of the NVI in the interval where it operates as an NDI that limits the usefulness of the NVI in the low velocity range (0.1–0.25 mm/μs). In this velocity range, values of τ in the neighborhood of 5 ns or more are required in order to obtain records with at least three or four fringes. This in turn leads to a greater averaging of the velocity measurements. Furthermore, elastic precursors causing velocity jumps of more than 0.1 mm/μs in a time less than τ cannot be detected because the early time NDI signal frequency may exceed the frequency response of the light detection system. This feature is described as lost fringes in the Valyn VISAR User's Handbook (VALYN VISAR, 1995).

Clearly, the NDI and VISAR principles described here indicate that there is a velocity range between 0.1–0.25 mm/μs over which particle velocities may not be measured with the desired accuracy. Barker and Hollenbach (1972) investigated the accuracy of the VISAR experimentally. They found that measurements with 2% accuracy can be obtained when a delay time of approximately 1 ns corresponding to a velocity per fringe constant equal to 0.2 mm/μs is used. Certainly, velocities below 0.2 mm/μs can be measured, but the uncertainty of the measurement increases because only a fraction of a fringe is recorded. In this case, signals in quadrature have to be recorded immediately before the experiment and *assume* the amplitude remains the same during the experiment (VALYN VISAR DATA REDUCTION PROGRAM, 1995). It should be pointed that the VISAR data reduction is very sensitive to the position and shape of the Lissajous (VALYN VISAR DATA REDUCTION PROGRAM, 1995). In both interferometers it might appear that sophisticated light detection systems having several GHz of bandwidth are required. Such systems although currently attainable remain for the most part prohibitively expensive.

Espinosa et al. (1997a) introduced a variable sensitivity displacement interferometer (VSDI) to provide an alternative to the NDI, and VISAR interferometers as applied to plate impact experiments, particularly within the noted velocity range of 0.1–0.25 mm/μs. The sensitivity of such an interferometer is fully variable; thus, it can operate over a wide range of particle velocities without exceeding the frequency response of the light detection system. Moreover, the VSDI system eliminates the need for very expensive optical components and ultra-fast oscilloscopes.

The methods discussed thus far represent the primary optical tools used to measure the surface motion in plate impact/shock wave experiments. Additional optical techniques for measuring the surface displacements of solids have been successfully developed and applied in other disciplines of scientific research. Most notably, in the field of ultrasonic detection, in-plane and out-of-plane surface displacements have been measured by high speed Holographic techniques (Wagner, 1986) differential laser Doppler anemometry (McKie and Wagner, 1988) and heterodyne speckle interferometry (Dandliker and Willemin, 1981). Recently, Cand et al. (1994) introduced a technique for simultaneous detection of in-plane and out-of-plane ultrasonic displacements through a two-channel confocal Fabry–Perot interferometer. The accuracy of the technique was examined by measuring the surface displacements associated with Rayleigh surface waves generated by a Q-switched Nd:YAG laser and found to be quite satisfactory. Despite its reliability and acceptance as a tool in the measurement of ultrasonic displacements, the Fabry–Perot interferometer has not found widespread use in plate impact/shock wave studies due to its relatively high photon fill time (Johnson and Burgess, 1968). This characteristic response time limits the resolution of the interferometer in the same way a long delay time, τ, limits the resolution of the VISAR.

A common feature of all interferometers discussed in this section is that successful signal acquisition requires good fringe contrast during the time of the experiment. Contrast losses arise from two main causes, interferometer imperfections and target motion (displacement and tilt). These losses can be in general time varying. For instance, a beam splitter that does not split light equally will produce a constant loss of contrast, while unevenly curved surfaces will produce a variable contrast change as a function of the light path in the interferometer. Target rotations that change the light path can be very detrimental to most interferometers. In this respect, interferometers that use scatter light from the target and fiber optics to transfer the laser light will minimize the loss in fringe contrast because the light path in the interferometer is fixed. Furthermore, even target rotations of a few milliradians will not result in signal loss in such systems. By contrast, standard interferometer set ups, without fiber optics, require tilts smaller than 1 mrad to avoid a change in the light path that can offset the beam from the optical components of the interferometer. This feature is particularly relevant in 2-D and 3-D wave propagation problems, e.g., penetration experiments, in which significant surface rotations are expected at diagnostic points. Recently, Barker developed a VISAR with these features (VALYN VISAR, 1995).

2.1. Variable sensitivity displacement interferometer theory

In this section we cover the theory of the VSDI as an example. An analysis of the VSDI sensitivity is provided and the equations used in the data reduction of recorded signals are derived.

To examine the governing equation for a variable sensitivity displacement interferometer, consider the effect of interfering a normally reflected beam with a beam diffracted at an angle θ with respect to the specimen normal as shown in Fig. 3. The normally reflected beam is split at beam splitter BS1. Each half of the normal beam is then made to interfere with one of the diffracted beams via beam splitters BS2 and BS3. The resulting signals generated by each interfering beam pair are monitored by photodetectors. The combined field for either pair of interfering plane waves leads to a classical interference expression of the form

$$I(t) \propto I^0 + I^{\pm} + 2\sqrt{(I^0 I^{\pm})}\cos(\beta)\cos\Psi^{\pm}(t). \tag{1}$$

Here, I^0 and $I^{\pm}$ represent the time averaged intensities of the respective contributing light fields and β is the angle between their respective polarization vectors. Normal and transverse particle motion introduce frequency modulation through the time varying phase term, namely,

$$\Psi^{\pm}(t) = \frac{2\pi}{\lambda}\left[2U\left(t-\frac{l^0}{c}\right) - U\left(t-\frac{l^{\pm}}{c}\right)(1+\cos\theta) \mp V\left(t-\frac{l^{\pm}}{c}\right)\sin\theta + (l^0 - l^{\pm})\right] + \phi^0 - \phi^{\pm}, \tag{2}$$

where λ is the wavelength of the laser source, $U(t)$ and $V(t)$ represent the normal and in-plane displacements of the point of observation from its position at time $t=0$; ϕ^+, ϕ^- represent constant arbitrary phase terms; and l^+, l^-, and l^0 represent the fixed initial path lengths traversed from target to detector by the $\theta^{\pm}$ diffracted beams and the normally reflected beam, respectively. Observe that the transverse motion phase term is subtracted for the case where the θ^+ beam is employed and otherwise added when interfering with the θ^- beam. Next, setting $l^0 = l^+ = l^-$ leads to a more simplified and useful form, i.e.,

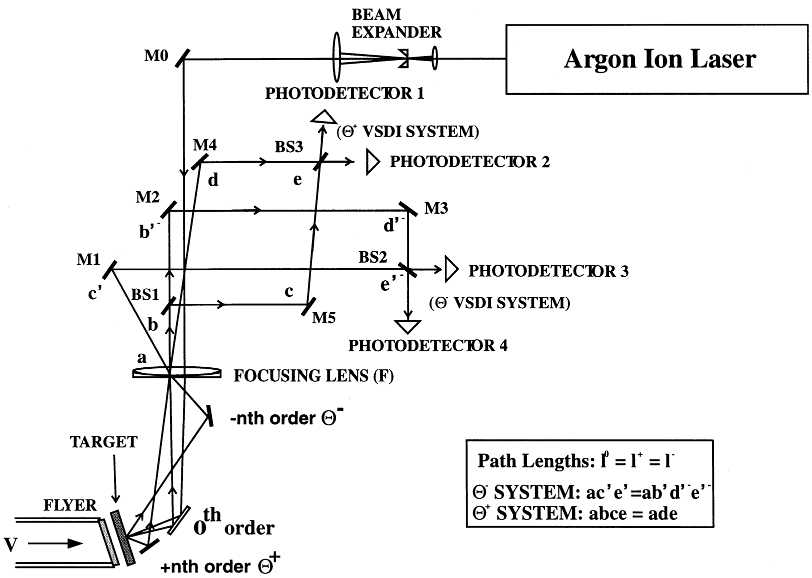

Fig. 3. Schematic of VSDI system. The $\Theta^{\pm}$ VSDI system is obtained by combining a normally reflected beam and a diffracted beam at an angle $\theta^{\pm}$. In this figure, mirrors M0–M5 and beam splitters BS1–BS3 are used to obtain the VSDI systems. The lens with focal length F is used to focus the beam at the grating plane in the anvil back surface.

$$\Psi^{\pm}(t) = \frac{2\pi}{\lambda}\left[U\left(t-\frac{l}{c}\right)(1-\cos\theta) \mp V\left(t-\frac{l}{c}\right)\sin\theta\right] + \phi^0 - \phi^{\pm}. \quad (3)$$

Eq. (3) shows that each VSDI system will generate a different signal frequency when used to monitor the same given combined state of motion. This effect is confirmed in pressure shear experiments at the time corresponding to the arrival of the shear wave at the target rear surface. With the delayed arrival of the shear wave, the signal now represents a linear combination of the two motion components. Consequently, the signal frequency is altered as indicated by Eq. (3), and each VSDI system exhibits a sudden increase or decrease depending upon whether the θ^+ or θ^- beam is being interfered.

Case of purely normal motion: (Desensitized normal displacement interferometer, DNDI). For $V(t) = 0$, a full fringe shift associated with a normal displacement δU satisfies

$$\Delta\Psi(t) = \frac{2\pi}{\lambda}[\delta U(t-l/c)](1-\cos\theta) = 2\pi. \quad (4)$$

Rearrangement of this expression and use of the grating equation, $d\sin\theta = n\lambda$, $n = \pm 1, 2, \ldots$, gives the fringe constant relation

$$\frac{\text{normal displacement}}{\text{fringe}} = \frac{\lambda}{1-\cos\theta} = \frac{\lambda}{1-\sqrt{1-(n\lambda\sigma)^2}}, \quad (5)$$

where $\sigma = 1/d$ represents the frequency of the diffraction grating and θ is used for $\theta^{\pm}$ since both the Θ^+ and Θ^- VSDI systems will function as identical desensitized normal displacement interferometers. The fringe constant varies from infinity at $\theta = 0°$ to λ [mm/fringe] at $\theta = 90°$. Therefore, a variable sensitivity displacement interferometer is obtained which is particularly well suited for normal plate impact experiments with particle velocities in excess of 100 m/s. Clearly, the selection of the appropriate angle θ should be based upon some a priori knowledge of the frequency range that will be spanned.

Case of purely in-plane motion: (Desensitized transverse displacement interferometer, DTDI). Referring to Eq. (3), we may consider the case where $U(t) = 0$, i.e., the case of pure in-plane motion. In this case, the variable phase is

$$\Psi(t)^{\pm} = \frac{2\pi}{\lambda}\left[\mp V\left(t-\frac{l}{c}\right)\sin\theta\right] + \phi^0 - \phi^{\pm} \quad (6)$$

and the Θ^+ and Θ^- VSDI systems now act as identical transverse displacement interferometers. A full fringe shift associated with a transverse displacement δV corresponds to

$$\delta\Psi(t) = \frac{2\pi}{\lambda}\left[\delta V\left(t-\frac{l}{c}\right)\sin\theta\right] = 2\pi \quad (7)$$

which may be rearranged and combined with $d\sin\theta = n\lambda$ to give the fringe constant relation

$$\frac{\text{transverse displacement}}{\text{fringe}} = \frac{\lambda}{\sin\theta} = \frac{1}{\sigma n}. \quad (8)$$

The DTDI sensitivity ranges from a complete loss of sensitivity at $\theta = 0°$ to a theoretical sensitivity limit of λ [mm/fringe] at $\theta = 90°$. The interferometer is "desensitized" in the sense that, for the same diffraction orders, it exhibits one-half the sensitivity of the TDI (Kim et al., 1977).

Case of combined normal and in-plane motions: (VSDI system). When the material point exhibits both normal and in-plane components of displacement, frequency modulation results through a linear combination of both motion components as dictated by Eq. (3). Decoupling of the two motions can be achieved by adding or subtracting the time varying phase terms of the Θ^+ and Θ^- VSDI signals. Addition provides an expression for a new phase term associated solely with a normal displacement U given by

$$\Psi(t)^+ + \Psi(t)^- = \frac{4\pi}{\lambda}U\left(t-\frac{l}{c}\right)(1-\cos\theta) + 2\phi_0 - \phi^- - \phi^+. \quad (9)$$

Hence, the fringe constant relation of this new signal is

$$\frac{\text{normal displacement}}{\text{fringe}} = \frac{\lambda}{2(1-\cos\theta)}. \quad (10)$$

It should be noted that this sensitivity is twice the sensitivity obtained by a single VSDI system for the case of pure normal motion, basically, because the signal obtained by addition of two VSDI systems exhibits a double recording of the normal displacement. By subtracting the phase terms of the Θ^+ and Θ^- VSDI signals, an expression for a phase term associated solely with an in-plane motion V is obtained, viz.,

$$\Psi(t)^- - \Psi(t)^+ = \frac{4\pi}{\lambda} V\left(t - \frac{l}{c}\right) \sin\,\theta - \phi^- + \phi^+. \tag{11}$$

The fringe constant of this new signal is given by

$$\frac{\text{transverse displacement}}{\text{fringe}} = \frac{\lambda}{2\sin\,\theta}. \tag{12}$$

This sensitivity is the same as the one exhibited by the TDI (Kim et al., 1977). This result is not surprising since the signal obtained by subtracting the two VSDI systems eliminates the effect of the normally reflected beam. We can conclude that this resulting signal is nothing other than a TDI signal.

An alternative approach for determining the normal and in-plane motions is to use the phase information of both a TDI system and a Θ^-VSDI system. For instance, by subtracting the time varying phases of a Θ^-VSDI system and a TDI system we obtain an expression for a phase term associated solely with the normal displacement $U(t)$, namely,

$$2\Psi(t)_{\Theta^-\mathrm{VSDI}} - \Psi(t)_{\mathrm{TDI}} = \frac{4\pi}{\lambda} U\left(t - \frac{l}{c}\right)(1 - \cos\,\theta) + \phi_0 - \phi_{\mathrm{TDI}} - \phi_{\Theta^-\mathrm{VSDI}}. \tag{13}$$

This equation shows once more that the normal motion can be recorded with the sensitivity given by Eq. (10). The in-plane motion V can be directly obtained from the TDI signal (Kim et al., 1977).

2.2. Example: Pressure–shear recovery experiment

We next present results obtained with the VSDI system applied to pressure–shear recovery experiments. The pressure–shear soft-recovery experiment (Espinosa et al., 1997a; Espinosa, 1996; Espinosa et al., 1995) is particularly suitable to investigate the applicability of the variable sensitivity displacement interferometer because normal velocities in the range 0.1–0.3 mm/μs need to be recorded. The configuration is shown in Fig. 1(a). The elastic wave fronts for a plane wave analysis of a high strain rate pressure–shear recovery experiment are given in a Lagrangian *X–t* diagram in Fig. 1(b).

In the present study the multi-plate impactor and target plates were made of speed-star steel (AISI type M2 tool steel) (Smith, 1993). The plates were lapped flat using a lapping machine and 15 μm alumina powder. A flatness better than 3 rings was measured by means of a Newton interferometer.

The specimen consisted of a woven glass fiber-reinforced polyester (GRP), 0.31 mm thick, glued to the two steel plates in the periphery. A sample density $\rho = 1.952 \pm 0.036$ Kg/m^3 and a longitudinal ultrasonic wave speed of 3.21 ± 0.01 Km/s were measured for this material (Chou and DeLuca, 1993). The composite material was found to be transversely isotropic. Measured independent elastic stiffness constants were $C_{11} = 31.55 \pm 3.8$ GPa, $C_{12} = 15.86 \pm 4.53$ GPa, $C_{13} = 9.75 \pm 3.83$ GPa, $C_{33} = 20.12 \pm 0.4$ GPa, $C_{44} = 4.63 \pm 1.22$ GPa, $C_{66} = 4.94 \pm 1.31$ GPa.

The multi-plate impactor, 57 mm in diameter, was made of two speed-star steel plates 3.3 and 2.4 mm thick, respectively, bonded by a 1 μm thick polymer film. The speed-star target plate was 6.45 mm thick, see Fig. 1(a).

The impactor was glued to the front end of a fiber glass tube with the impact plane skewed from the axis of the tube at an angle of 18°. An aluminum back with two rubber O-rings was mounted in the rear end of the tube to seal the wrap-around breech. A key was mounted on the middle of the fiber glass tube to prevent rotation of the projectile. The projectile velocity was measured, just before impact, by recording the times of contact of four wire pins placed in the path of the projectile. An impact velocity of 0.132 mm/μs was measured in the experiment.

A grating with 1000 lines/mm was manufactured in the 6.45 mm-thick target plate back surface to produce the desired diffracted beams. The target plate was mounted in a holder ring and aligned to the impactor surface within 0.5 mrad using the optical technique developed by Kumar and Clifton (1977). In order to check the angle of misalignment at impact, the times of contact at four voltage-biased pins were recorded.

Through a logical circuit, contact of the four pins gave four voltage steps, in the ratio of 1:2:4:8, which were recorded in an oscilloscope. A tilt of 1.5×10^{-3} rad was measured in the experiment.

A combined Θ^- VSDI–TDI system was utilized to monitor the normal and transverse velocities at the target free surface. The zero order reflected beam was combined with the negative first order diffracted beam to produce a Θ^- VSDI system. A TDI interferometer was obtained by mixing the two first order diffracted beams (Kim et al., 1977). Additional details of the experimental procedure are given in (Espinosa et al., 1997a; Espinosa et al., 1995).

The signals produced by the combined Θ^- VSDI–TDI system, were recorded in a Tektronix DSA 602A oscilloscope. Decoupling between the normal and in-plane motions was accomplished by first obtaining the in-plane motion, V, directly from the TDI signal and then the normal motion, U, from Eq. (13). To eliminate electronic noise, the interference fringes were filtered using a fast-Fourier transform method and a cut-off frequency higher than the maximum fringe frequency. Furthermore, since the signal amplitude does not contain displacement information, it is customary to scale the signal to a constant amplitude prior to the displacement calculation. Hence, the filtered fringes were then scaled to obtain uniform fringe amplitude.

Based on the displacement interferometer principles, one can assume that the interferometer signal consists of fringes in a sine-like function of voltage versus time, e.g., $y(t) = a(t)\sin(f(t)) + b(t)$, where $a(t)$ is the amplitude, $b(t)$ is the zero offset, and $f(t)$ is the phase function. In general, $a(t)$ and $b(t)$ are not constant. They can be evaluated by finding the envelopes, $h(t)$ and $l(t)$, formed by peaks and valleys, respectively. These functions are given by $a(t) = 0.5(h(t) - l(t))$ and $b(t) = 0.5(h(t) + l(t))$. The amplitude corrected signal, $y_0(t)$, is then determined by $y_0(t) = (y(t) - b(t))/a(t)$. The signal phase function can be obtained from $f(t) = \arcsin(y_0(t))$. Then the displacement can be computed from $d(t) = d_0 f(t)/2\pi$. The constant d_0 is a function of the interferometer and is defined by Eqs. (10) and (12) for the VSDI and TDI systems, respectively.

Velocities were obtained by differentiating the displacement histories numerically. All the calculations were automatically performed with MATLAB. The functions MENU, GINPUT, INPUT, and STRCMP were used to input the data files. The functions FIR1 and FFTFILT were used to performed the fast Fourier transform filtering. The function INTERP1 was employed to fit the peaks and valleys with cubic splines. The function GRADIENT was utilized to perform the numerical differentiation.

The normal velocity-time profiles obtained from the experiment and the amplitude corrected signal are plotted in Fig. 4. Upon arrival of the normal wave, fringes are produced in the Θ^- VSDI channel. A significant frequency increase is observed after arrival of the shear wave in accordance with Eq. (3). The normal velocity exhibits a jump in velocity to a level of approximately 0.05 mm/μs followed by a reduction and increase in velocity due to wave reverberations in the thin polymer layer used in the multi-plate flyer. An approximately constant velocity of 0.095 mm/μs is monitored in the next 1.8 μs which is in agreement with the elastic prediction.

The transverse velocity history together with the amplitude corrected TDI signal are shown in Fig. 5. The transverse particle velocity progressively increases to a maximum value of about 0.019 mm/μs corresponding to a shear stress of 240 MPa. In high strain rate pressure–shear experiments, the recorded velocity at the target free sur-

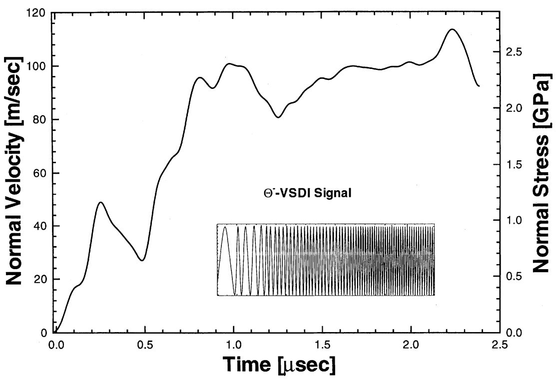

Fig. 4. Normal velocity–time profile from pressure–shear recovery experiment. The plotted time is after arrival of normal wave to the steel target plate back surface.

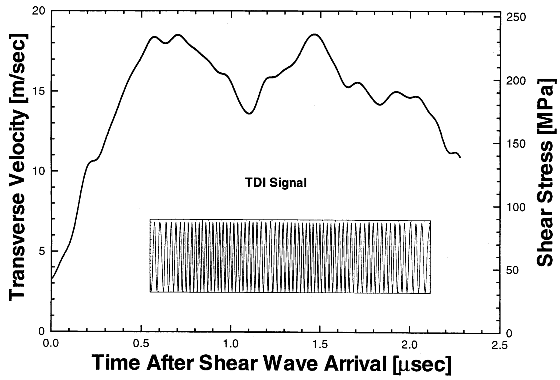

Fig. 5. Transverse velocity–time profile from pressure–shear recovery experiment. The plotted time is after arrival of shear wave to the steel target plate back surface.

face can be used in the calculation of stresses, at the target–specimen interface, using the method of characteristics (Espinosa and Clifton, 1991). In these calculations, a state of one dimensional elastic strain is assumed.

Small fluctuations in the normal and transverse velocity histories are due in part to errors in data reduction arising from the insensitivity of the VSDI and TDI at the peaks and valleys of the trace (Espinosa and Clifton, 1991).

In summary, this section has discussed several interferometric techniques which are commonly used in impact experiments. In particular, the theoretical analysis of a VSDI, obtained by interfering a normally reflected beam with a beam diffracted at an angle θ with respect to the specimen normal, was presented as an example. It is shown that in the VSDI a wide range of sensitivities can be obtained by changing the angle between the two beams. In principle, the VSDI interferometer presented here can be used in wave propagation experiments conducted on metallic and nonmetallic materials in a variety of impact configurations including those in which an optical window is employed.

3. In-material stress and velocity measurement techniques

Several research efforts have been made for *inmaterial measurements* of longitudinal and shear waves in dynamically loaded solids. Gupta (1976), Young and Dubugnon (1977), and Gupta et al. (1980) reported successful experiments where velocity histories have been obtained at interior surfaces by inserting metallic gauges in a magnetic field and measuring the current generated by their motion; these are called electromagnetic particle velocity (EMV) gauges. This technique can be applied only to nonmetallic materials.

Another technique developed for in-material measurements (Williams and Keough, 1968; Rosenberg and Bless, 1986), employs manganin gauges placed between the specimen and a back plate, to measure the time history of the longitudinal stress, or by placing a manganin gauge at an interface made in the direction of wave propagation, to measure lateral stresses. In this configuration the dynamic shear resistance of the material can be obtained by simultaneously measuring the axial and lateral stresses.

An alternative technique for the in-material measurement of the dynamic shear resistance of materials, is the use of oblique impact with the specimen backed by a window plate (Espinosa, 1996). In this technique longitudinal and shear wave motions are recorded by a combined NDI, or an NVI (Barker and Hollenbach, 1965), and a TDI (Kim et al., 1977). Alternatively, the VSDI interferometer previously discussed can be used. The velocity measurements are accomplished by manufacturing a high pitch diffraction grating at the specimen–window interface (Espinosa, 1996).

3.1. In-material stress measurements with embedded piezoresistant gauges

Many materials exhibit a change in electrical resistivity as a function of both pressure and temperature. Manganin, an alloy with 24 wt% Cu, 12 wt% Mn, and 4 wt% Ni, was first used as a pressure transducer in a hydrostatic apparatus by Bridgman (1911). Manganin is a good pressure transducer because it is much more sensitive to pressure than temperature changes. Impact experiments performed by Bernstein and Keough (1964), and DeCarli et al. (1976) show a linear relationship between axial stress σ_1, in the direction of wave propagation, and resistance change.

Namely, $\sigma_1 = \Delta R/kR_0$ in which R_0 is the initial resistance and k is the piezoresistance coefficient. For manganin, DeCarli et al. (1976), found $k = 2.5 \times 10^{-2}$ GPa^{-1}. The value of this coefficient is a function of the gauge alloy composition, therefore, a calibration is required. Manganin gauges are well suited for stress measurements above 4 GPa and up to 100 GPa. At lower stresses, carbon and ytterbium have a higher pressure sensitivity (Chhabildas and Graham, 1987) resulting in larger resistance changes and hence more accurate measurements. Carbon gauges can be accurately used up to pressures of 2 GPa while ytterbium can be used up to pressures of 4 GPa. Various types of manganin gauges are manufactured by Measurements Group. Ytterbium and Carbon gauges are manufactured by Dynasen.

In plate impact experiments, the gauge element is usually embedded between plates to measure either longitudinal or transverse axial stresses. A schematic of the experimental configuration is shown in Fig. 6. If the gauge is placed between conductive materials, it needs to be electrically insulated by packaging the gauge using mylar, mica or teflon. Another reason for using a gauge package is to provide additional protection in the case of brittle materials undergoing fracture.

Through the use of metallic leads, the gauge is connected to a power supply that energizes the gauge prior to the test. The power supply comprises a capacitor that is charged to a selected voltage and discharged upon command into a bridge network by the action of a timer and a power transistor. The current pulse that is delivered to the bridge is quasi-rectangular with a duration between 100 and 800 μs. The bridge network is basically a Wheatstone bridge that is externally completed by the gauge. The gauge which is nominally 50 Ω, is connected to the bridge with a 50 Ω coaxial cable. The reason for using a pulse excitation of the bridge, rather than a continuous excitation, is that such approach permits high outputs without the need for signal amplification and avoids excessive Joule heating effects that can result in gauge failure. The bridge output is connected to an oscilloscope for the recording of voltage changes resulting from changes in resistance. The relation between voltage and resistance change is obtained by means of a calibration with a variable resistor. A compensating bridge with these characteristics is presently manufactured by Dynasen.

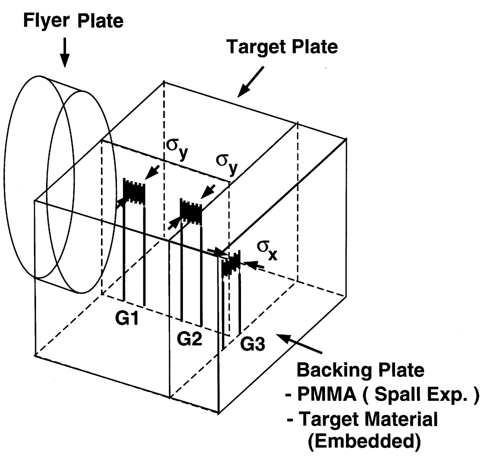

Fig. 6. Manganin gauge experimental configuration. Gauges G1 and G2 record the transverse stress. Gauge G3 records the longitudinal stress at the specimen–back plate interface.

A concern with this technique is the perturbation of the one dimensionality of the wave propagation due to the presence of a thin layer, perpendicular to the wave front, filled with a material having a different impedance and mechanical response. Calculations by Wong and Gupta (1991) show that the inelastic response of the material being studied affects the gauge calibration. Recently, Rosenberg and Brar (1994) reported that in the elastic range of the gauge material its resistance change is a function of the specimen elastic moduli. In a general sense, this is a disadvantage in the lateral stress gauge concept. Nonetheless, their analysis shows that in the plastic range of the lateral gauge response, a single calibration curve for all specimen materials exists. These findings provide a methodology for the appropriate interpretation of lateral gauge signals, and increase the reliability of the lateral stress measuring technique.

3.2. Example: Identification of failure waves in glass

In-material axial and transverse stress measurement have been successfully used in the interpretation of the so-called failure waves in glass

(Brar and Bless, 1992; Espinosa, Xu and Brar, 1997). By using the configuration shown in Fig. 6 with the longitudinal gauge backed by a PMMA plate, the dynamic tensile strength of the material was determined. In these experiments, manganin gauges type LM-SS-125CH-048 manufactured by Measurements Group, were used. Soda-lime and Corning 1723 aluminosilicate glass plates were tested. The density and longitudinal wave velocity for the soda-lime glass were 2.5 g/cm^3 and 5.84 mm/μs, respectively. The aluminosilicate glass properties were: density = 2.64 g/cm^3, Young's modulus = 86 GPa, and Poisson's ratio = 0.24.

By appropriate selection of the flyer plate thickness, the plane at which tension occurs for the first time within the sample was located close to the impact surface or close to the specimen–PMMA interface. In experiment (7-0889) we impacted a 5.7-mm thick soda-lime glass target with a 3.9 mm aluminum flyer at a velocity of 906 m/s. The manganin gauge profile is shown in Fig. 7. The spall plane in this experiment happened to be behind the failure wave. The profile shows the arrival of the compressive wave with a duration of approximately 1.5 μs, followed by a release to a stress of about 3 GPa and a subsequent increase to a constant stress level of 3.4 GPa. The stress increase after release is the result of reflection of the tensile wave from material that is being damaged under dynamic tension and represents the dynamic tensile strength of the material (spall strength). From this trace we conclude that soda-lime glass shocked to a stress of 7.5 GPa has a spall strength of about 0.4 GPa behind the so-called failure wave. We repeated this experiment with a 2.4-mm thick aluminum flyer (7-1533) and found complete release from the back of the aluminum impactor, see Fig. 7. A pull back signal is observed after approximately 0.45 μs with a rise in stress of about 2.6 GPa. It should be noted that the spall plane in this experiment was in front of the failure wave. These two experiments clearly show that the spall strength of glass depends on the location of the spall plane with respect to the propagating failure wave. For soda-lime glass a dynamic tensile strength of 2.6 and 0.4 GPa are measured with manganin gauges in front and behind the failure wave, respectively. Similar results were obtained by Dandekar and Beaulieu (1995) using a VISAR.

Additional features of the failure wave phenomenon were obtained from transverse gauge experiments performed on soda-lime and aluminosilicate glasses (Espinosa et al., 1997). In these experiments one or two narrow, 2 mm wide, manganin gauges (Type C-8801113-B) were embedded in the glass target plates in the direction transverse to the shock direction as shown in Fig. 6. A thick back plate of the same glass was used in the target assembly. Aluminum or glass impactor plates were used to induce failure waves. The transverse stress, σ_2, was obtained from the transverse gauge record. Fig. 8 shows measured transverse gauge profile at

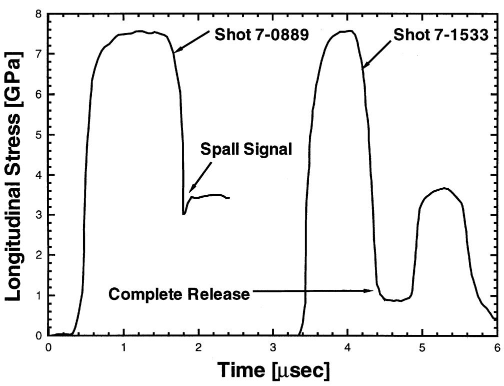

Fig. 7. Gauge profile from experiment 7-0889 showing reduced spall strength. Gauge profile from experiment 7-1533 showing complete release and a spall strength of 2.6 GPa.

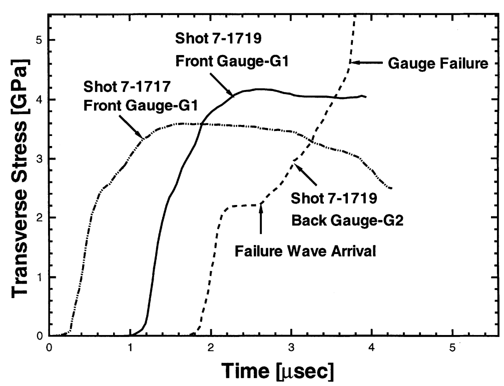

Fig. 8. Manganin gauge records from shots 7-1717 and 7-1719, showing transverse stress histories at two locations (see Fig. 6 for location of transverse gauges).

Table 1
Summary of experimental data using manganin gauges

Shot no.	Material	Impactor/thickness (mm)	Target/thickness (mm)	Impact velocity (m/s)	Normal stress (GPa)
7-0889	Soda-lime	Al/3.9	SLG/5.7	906	7.5
7-1533	Soda-lime	Al/2.4	SLG/5.7	917	7.6
7-1717	C-1723	Al/12.7	CG/19.4	770	6.1
7-1719	C-1723	Al/14.5	CG/19.4	878	6.97

two locations (shot-7-1719) in the Corning 1723 glass. One can clearly see the two wave structure which results from the failure wave following the longitudinal elastic wave. The first gauge, at the impact surface, shows an increase in lateral stress to the value predicted by 1-D wave theory, 2.2 GPa in Fig. 8, immediately followed by a *continuous* increase to a stress level of 4.2 GPa. The second gauge, at 3 mm from the impact surface, initially measures a constant lateral stress of 2.2 GPa followed by an increase in stress level on arrival and passage of the failure wave. It should be noted that gauge G1 records a continuous increase in lateral stress up to 4.26 Pa. This can only be the case if the failure wave has an incubation time of less than 250 ns. By contrast, gauge G2 sees the arrival of the failure wave about 700 ns after the arrival of the elastic wave (see step at 2.2 GPa). Furthermore, these traces also confirm that the failure wave initiates at the impact surface and propagates to the interior of the sample. This interpretation is in agreement with the impossibility of monitoring impact surface velocity with a VISAR system (Dandekar and Beaulieu, 1995) when failure waves are present.

The impact parameters used in the above experiments are summarized in Table 1. Measured profiles of manganin gauges were converted to stress–time profiles following the calibrations of longitudinal and transverse manganin gauges under shock loading given in Rosenberg and Partom (1985) and Rosenberg and Brar (1994), respectively.

References

Barker, L.M., Hollenbach, R.E., 1965. Interferometer technique for measuring the dynamic mechanical properties of materials. Rev. Sci. Instr. 36 (11), 1617–1620.

Barker, L.M., Hollenbach, R.E., 1972. Laser interferometry for measuring high velocities of any reflecting surface. J. Appl. Phys. 43 (11), 4669–4675.

Bernstein, D., Keough, D.D., 1964. Piezoresistivity of manganin. J. Appl. Phys. 35, 1471.

Brar, N.S., Bless, S.J., 1992. Failure waves in glass under dynamic compression. High Pressure Research 10, 773–784.

Bridgman, P.W., 1911. Proc. Amer. Acad. Arts Sci. 47, 321.

Cand, A., Monchalin, J.-P., Jia, X., 1994. Detection of in-plane and out-of-plane ultrasonic displacements by a two-channel confocal Fabry–Perot interferometer. Appl. Phys. Lett. 64, 414.

Chhabildas, L.C., Sutherland, H.J., Asay, J.R., Jr., 1979. A velocity interferometer technique to determine shear-wave particle velocity in shock-loaded solids. J. Appl. Phys. 50 (8), 5196–5201.

Chhabildas, L.E., Graham, R.A., 1987. Techniques and theory of stress measurements for shock-wave applications. Appl. Mech. Div. ASME AMD-83, 1–18.

Chou, S.C., DeLuca, E., 1993. Dynamic response of S-2 glass reinforced plastic structural armor. Report No. ARL-SR-5.

Clifton, R.J., 1970. Analysis of the laser velocity interferometer. J. Appl. Phys. 41 (13), 5335–5337.

Clifton, R.J., Klopp, R.W., 1985. Pressure–shear plate impact testing. Metals Handbook: Mechanical Testing 8. Ninth ed., p. 230.

Dandekar, D.P., Beaulieu, P.A., 1995. Failure wave under shock wave compression in soda lime glass. In: Murr, L.E., et al. (Eds.), Metallurgical and Material Applications of Shock-Wave and High-Strain-Rate Phenomena, Elsevier, Amsterdam.

Dandliker, R., Willemin, J.-F., 1981. Measuring microvibrations by heterodyne speckle interferometry. Opt. Lett. 6, 165.

DeCarli, P.S., Erlich, D.C., Hall, L.B., Bly, R.G., Whitson, A.L., Keough, D.D., Curran, D., 1976. Stress-gauge system for the megabar (100 MPa) range. Report No. DNA 4066F, Defense Nuclear Energy, SRI Intl., Pal Alto, CA.

Espinosa, H.D., Clifton, R.J., 1991. Plate impact experiments for investigating inelastic deformation and damage of advanced materials. In: Kim, K.S. (Ed.), Symposium on Experiments in Micromechanics of Fracture-Resistant Materials (ASME Winter Annual Meeting), Atlanta, GA, pp. 37–56.

Espinosa, H.D., 1992. Micromechanics of the dynamic response of ceramics and ceramic composites. Ph.D. Thesis, Brown University, Providence, RI.

Espinosa, H.D., Raiser, G., Clifton, R.J., Ortiz, M., 1992. Performance of the star-shaped flyer in the study of brittle materials: Three dimensional computer simulations and experimental observations. J. Appl. Phys. 72 (8), 3451–3457.

Espinosa, H.D., Emore, G., Xu, Y., 1995. High strain rate behavior of composites with continuous fibers. In: Rajapakse, Y.D.S., Vinson, J.R. (Eds.), ASME Special Technical Publication, High Strain Rate Effects on Polymer, Metal and Ceramic Matrix Composites and Other Advanced Materials. ASME, San Francisco, CA, pp. 6–16.

Espinosa, H.D., 1996. Dynamic compression-shear loading with in-material interferometric measurements. Rev. Sci. Instr. 67 (11), 3931–3939.

Espinosa, H.D., Xu, Y., Brar, N.S., 1997. Micromechanics of failure waves in glass: Experiments. J. Amer. Cer. Soc. 80 (8), 2061–2073.

Espinosa, H.D., Mello, M., Xu, Y., 1997a. A variable sensitivity displacement interferometer with application to wave propagation experiments. J. Appl. Mech. 64, 123–131.

Gupta, Y.M., 1976. Shear measurements in shock loaded solids. Appl. Phys. Lett. 29, 694–697.

Gupta, Y.M., Keough, D.D., Walter, D.F., Dao, K.C., Henley, D., Urweider, A., 1980. Experimental facility to produce and measure compression and shear waves in impacted solids. Rev. Sci. Instr. 51 (a), 183–194.

Hemsing, W.F., 1979. Velocity Sensing Interferometer (VISAR) modification. Rev. Sci. Instr. 50 (1), 73–78.

Johnson, P.M., Burgess, Y.J., 1968. Free surface velocity measurement of an impacted projectile by optical Doppler shift. Rev. Sci. Instr. 39, 1100.

Kumar, P., Clifton, R.J., 1977. Optical alignment of impact faces for plate impact experiments. J. Appl. Phys. 48 (3), 1366–1367.

Kumar, P., Clifton, R.J., 1979. Dislocation motion and generation in LiF single crystals subjected to plate-impact. J. Appl. Phys. 50 (7), 4747–4762.

Kim, K.-S., Clifton, R.J., Kumar, P., 1977. A combined normal and transverse displacement interferometer with an application to impact of Y-cut quartz. J. Appl. Phys. 48 (10), 4132–4139.

Machcha, A.R., Nemat-Nasser, S., 1994. Pressure–shear recovery experiments. Mech. Mater. 18, 49–53.

Machcha, A.R., Nemat-Nasser, S., 1996. Effects of geometry in pressure–shear and normal plate impact experiments: Three-dimensional finite element simulations and experimental observations. J. Appl. Phys. 80 (6), 3267–3274.

McKie, A.D.W., Wagner, J.W., 1988. Optical sensing of in-plane ultrasonic transients. Appl. Phys. Lett. 53, 1043.

Ramesh, K.T., Clifton, R.J., 1987. A pressure–shear plate impact experiment for studying the rheology of lubricants at high pressures and high strain rates. J. Tribology 109, 215.

Rosenberg, Z., Partom, Y., 1985. Longitudinal dynamic stress measurements with in-material piezoresistive gauges. J. Appl. Phys. 58, 1814.

Rosenberg, Z., Bless, S.J., 1986. Determination of dynamic yield strengths with embedded manganin gages in plate-impact and long-rod experiments. Exp. Mech., 279–282.

Rosenberg, Z., Brar, N.S., 1994. Hysteresis of lateral piezoresistive gauges, high pressure science and technology. In: Schmidt, S.C. (Ed.), Joint AIRAPT-APS Conference, Colorado Springs, CO, pp. 1707–1710.

Smith, W.F., 1993. Structure and Properties of Engineering Alloys. McGraw-Hill, New York.

Sullivan, J.P., Ezekiel, S., 1974. A two-component laser Doppler velocimeter for periodic flow fields. J. Phys. E7, 272–274.

VALYN VISAR, 1995. User's Handbook, Valyn International, Alburquerque, New Mexico 87112-3771.

VALYN VISAR DATA REDUCTION PROGRAM, 1995. User's Handbook, Valyn International, Alburquerque, New Mexico 87112-3771.

Wagner, J.W., 1986. Mater. Eval. 44, 1238.

Williams, R., Keough, D.D., 1968. Piezoresistive response of thin films of calcium and lithium to dynamic loading. Bull. Amer. Phys. Soc. Series II 12, 1127.

Wong, M.K.W., Gupta, Y.M., 1991. Dynamic inclusion analyses of lateral piezoresistance gauges under shock wave loading. In: Schmidt, S.C., Dick, R.D., Forbes, J.W., Tasker, D.J. (Eds.), Shock Compression of Condensed Matter, Elsevier, Essex, UK.

Yadav, S., Davis, J.A., Ramesh, K.T., 1993. Damage and recovery experiments using pressure–shear plate impact. In: Experimental Techniques in the Dynamics of Deformable Solids, vol. 165. ASME AMD, pp. 71–78.

Young, Z., Dubugnon, O., 1977. A reflected shear-wave technique for determining dynamic rock strength. Int. J. Rock Mech. Min. Sci., 247–259.

Zhou, M., Needleman, A., Clifton, R.J., 1994. Finite element simulations of shear localization in plate impact. J. Mech. Phys. Solids 42 (3), 423–458.